Josip Bašić
Nastia Degiuli
Andreja Werner

SIMULATION OF WATER ENTRY AND EXIT OF A CIRCULAR CYLINDER USING THE ISPH METHOD

Summary

Simulations of free surface flows, as well as flows with moving boundaries in general, are quite difficult to describe with the classic, mesh-based Eulerian methods, such as finite difference, finite volume, and finite element methods. Meshless Lagrangian methods or a combination of Eulerian-Lagrangian methods that have the ability to describe the free surface with large deformations have been developing in the past fifteen years. In this paper, the Lagrangian incompressible smoothed particle hydrodynamics (ISPH) method for simulating the dynamics of an incompressible viscous fluid flow is presented. The ISPH method is an attractive choice for the simulation of incompressible fluid flow because it is based on the simple SPH formulations, and it solves the pressure field implicitly using the projection scheme of solving the Navier-Stokes equations. A computer code for the simulation of the viscous incompressible fluid flow based on the ISPH method is developed. Water entry and water exit of a rigid body are very important phenomena in marine hydrodynamics and there have been many studies and experiments on the topic. The cases of two-dimensional water entry and water exit of a circular cylinder at a forced constant velocity were studied in order to verify and validate the method. Numerical simulations of a rigid circular cylinder falling onto initially calm water at a constant entry velocity were carried out. Also numerical simulation of the water exit of a circular cylinder, initially fully immersed, was performed. The obtained numerical results are in good agreement with the experimental and analytical ones found in the literature.

Key words: incompressible smoothed particle hydrodynamics (ISPH) method, water entry, water exit, circular cylinder, free surface

1. Introduction

Numerical simulation has become an important tool for the solving of engineering problems, and the problems of fluid mechanics with free surface, which are of great importance. With the help of today's computer power which is rapidly developing, it is necessary to impose fewer assumptions, and problems can be solved with more requested details. Numerical simulations complement and replace to an extent expensive and complicated experiments. They require the translating of physical problems into a discrete

system of mathematical equations. In the case of fluid dynamics, it is a system of time and space-dependent partial differential equations. With a sufficient number of initial and boundary conditions and the specific discretization of space and time, a solution of the mentioned system can be found by numerical integration. There are several ways how to discretize partial differential equations and how to treat the free surface.

Traditional Eulerian methods with a fixed computational mesh have difficulties in describing the free surface, while meshless Lagrangian methods have a natural ability to describe this phenomenon in detail. Methods that combine the Eulerian mesh with particles, such as the Particle-in-Cell method and the Marker-and-Cell method, aim at overcoming the shortcomings of mesh-dependent methods. However, these methods suffer from excessive numerical diffusion or incorrect solution of nonlinear advection.

Numerical simulations of problems involving the free surface that use Lagrangian meshless (mesh-free) methods are becoming increasingly popular in practice. One subset of meshless methods comprises methods for particle systems that allow the simulation of problems with large deformations. There are no restrictions on the geometry of the system or how the system may evolve from initial conditions.

Smoothed Particle Hydrodynamics (SPH) is one of the oldest methods of the kind, presented by Lucy [1], Gingold and Monaghan [2] in 1977. It was developed due to the need to solve astrophysical problems. Lately, the SPH method has been developing rapidly and has become a unique tool for solving the problems of fluid dynamics thanks to its formalism that does not require a mesh and the possibility to support large deformations and morphological changes. However, SPH is a relatively new tool and it is not developed to the degree of the finite difference or the finite volume method, for example.

Traditionally, the SPH method, introduced by Monaghan [3, 4] through the equation of state, which depends on the density and the speed of sound in the considered medium, is applied on the assumption that the fluid is weakly compressible.

Weakly Compressible Smoothed Particle Hydrodynamics (WCSPH) is a completely explicit algorithm and easy to implement, but it has a number of disadvantages. Great sound velocity due to the restrictive Couran-Friedrichs-Lewy (CFL) criterion imposes a very small required time step, and the pressure fluctuates, which leads to numerical instability and non-smooth fields of hydrodynamic variables. In order to overcome these problems, Cummins and Rudman [5] presented an Incompressible Smoothed Particle Hydrodynamics (ISPH) method based on the implicit projection scheme to solve the Navier-Stokes equations. Results of verification tests showed that the ISPH method eliminates the difficulties encountered by WCSPH and gives more accurate predictions of velocity and pressure field.

Examples of practical engineering problems that are suitable for the simulation of the SPH method are e.g. intensive impacts of gravitational waves on structures. The current trend is to build structures, such as wind farms, on the sea at larger distances from the coast to gain advantage of a higher wind velocity and to avoid audible and visual problems. Such a structure is subjected to higher loads of gravitational waves. In addition to these structures, there is a range of other structures that are affected by the same problem such as oil platforms, fish farms, lighthouses, harbours, etc. Fast ships present another example where the "violent" interaction between the free surface and a solid construction plays an important role. Some of the relevant phenomena related to this topic are slamming and the wave pattern generated by the movement of the ship. Sloshing and green water on the deck of the ship are also examples of issues that are of great importance.

The aim of this paper is to implement the ISPH method as an attractive engineering tool with a code able to handle very large numbers of particles, using parallel computing to enable a wide range of applications.

2. Governing equations

The Navier-Stokes equations, i.e. conservation of momentum and continuity equation, are solved in Lagrangian form in the SPH method, as defined by equations (1) and (2), respectively. Equation (3) is also solved for the particle positions:

$$\frac{\mathrm{D}\vec{u}}{\mathrm{D}t} = -\frac{1}{\rho}\nabla p + \nu\nabla^2\vec{u} + \vec{g} \tag{1}$$

$$\nabla\cdot\vec{u} = 0 \tag{2}$$

$$\frac{\partial\vec{x}}{\partial t} = \vec{u} \tag{3}$$

where $\vec{u}$ is the particle velocity, p is the pressure, $\vec{g}$ is an external body force, ν is the kinematic viscosity, ρ is the density, t is the time and $\vec{x}$ is the particle position vector.

Material derivative $\mathrm{D}/\mathrm{D}t$ of a vector field $\vec{u}$ is defined by:

$$\frac{\mathrm{D}\vec{u}}{\mathrm{D}t} = \frac{\partial\vec{u}}{\partial t} + \left(\vec{u}\cdot\nabla\right)\vec{u} \tag{4}$$

Equation (2) represents the condition of incompressibility of the fluid derived from the continuity equation. Only for a small number of cases, i.e. for mostly fully developed flows in simple geometries, there exists a unique analytic solution. These special cases are essential foundations for the verification and validation of numerical methods that simulate fluid dynamics, but their practical application is limited.

Since particles move with the fluid, the material derivative of the velocity field is simply the time derivative of the velocity of particles meaning that the convective term $\left(\vec{u}\cdot\nabla\right)\vec{u}$ is not needed for particle systems.

2.1 Formulation of SPH equations

The basic SPH methodology is based on the description of any scalar field function f using an integral and the Dirac $\delta(x)$ function:

$$f(\vec{x}) = \int_{\Omega} f(\vec{x}\,')\delta\left(\left|\vec{x} - \vec{x}\,'\right|\right)\mathrm{d}\vec{x}\,' \tag{5}$$

where Ω is the fluid domain and $f(x)$ is the scalar function. $\delta(x)$ is the Dirac delta function, which can be described as a function whose value is always equal to zero except at the origin:

$$\delta(x) = \begin{cases} +\infty & \text{for } x = 0 \\ 0 & \text{for } x \neq 0 \end{cases} \tag{6}$$

Obviously, $\int_{-\infty}^{+\infty}\delta(x)\mathrm{d}x = 1$. Replacing the Dirac delta function with an appropriate kernel function, the function f can be approximated by the following expression:

$$f(\vec{x}) \approx \int_{\Omega} f(\vec{x}\,')w\left(\left|\vec{x} - \vec{x}\,'\right|, h\right)\mathrm{d}\vec{x}\,' \tag{7}$$

where $w\left(\left|\vec{x} - \vec{x}\,'\right|, h\right)$ is the kernel function, h is the smoothing length, the value that defines the domain of influence of the kernel function.

The gradient of the function f and the divergence of the function $\vec{f}$ can be respectively written as:

$$\nabla f(\vec{x}) \approx \int_{\Omega} f(\vec{x}')\nabla w\left(\left|\vec{x}-\vec{x}'\right|,h\right)\mathrm{d}\vec{x}' \tag{8}$$

$$\nabla \cdot \vec{f}(\vec{x}) \approx \int_{\Omega} \vec{f}(\vec{x}')\cdot\nabla w\left(\left|\vec{x}-\vec{x}'\right|,h\right)\mathrm{d}\vec{x}' \tag{9}$$

2.2 Particle discretization

In order to develop a practical numerical scheme, the fluid domain is discretized using the finite set of particles with properties such as mass, volume, pressure, and velocity vector. Particles are scattered in the fluid domain space and they can move independently. Practically, equation (7) in the position of particle a can be discretized with a sum which refers to all particles in the smoothing kernel domain except the observed particle a:

$$f_a \approx \sum_{b\in N} V_b f(\vec{x}_b)w\left(\left|\vec{x}_a-\vec{x}_b\right|,h_b\right) \tag{10}$$

$$f_a \approx \sum_{b\in N} V_b f(\vec{x}_b)w_{ab} \tag{11}$$

where $V_b = m_b/\rho_b$ is the volume of the neighbour particle b, and for the simplicity of writing $w_{ab} \equiv w\left(\left|\vec{x}_a-\vec{x}_b\right|,h_b\right)$. Analogously, it is possible to discretize equation (8) in the position of particle a in the following way:

$$\nabla f_a \approx \sum_{b\in N} V_b f(\vec{x}_b)\nabla w_{ab} \tag{12}$$

Expression (12) represents basic form of the SPH gradient operator. Equation (9) in the position of the particle a can be discretized as follows:

$$\nabla \cdot \vec{f}_a \approx \sum_{b\in N} V_b f(\vec{x}_b)\cdot\nabla w_{ab} \tag{13}$$

Expression (13) represents basic form of the SPH divergence operator.

It has been shown that use of basic forms of the SPH gradient and divergence operators can lead to simulation instability and inefficient convergence [6]. Alternative ways to describe a derivative of spatial function are given as:

$$\nabla f(\vec{x}) = \frac{1}{\rho}\left[\nabla\left(\rho f(\vec{x})\right)-f(\vec{x})\nabla\rho\right] \tag{14}$$

$$\nabla f(\vec{x}) = \rho\left[\nabla\left(\frac{f(\vec{x})}{\rho}\right)-\frac{f(\vec{x})}{\rho^2}\nabla\rho\right] \tag{15}$$

which can be written in the SPH form as follows:

$$\nabla f_a \approx \frac{1}{\rho_a}\sum_{b\in N} m_b\left[\left(f(\vec{x}_b)\right)-f(\vec{x}_a)\right]\nabla w_{ab} \tag{16}$$

$$\nabla f_a \approx \rho_a \sum_{b \in N} m_b \left[\frac{f(\vec{x}_a)}{\rho_a^2} + \frac{f(\vec{x}_b)}{\rho_b^2} \right] \nabla w_{ab} \tag{17}$$

Equation (16) has a symmetric, and equation (17) has an asymmetric form, as seen when particles *a* and *b* swap places. The asymmetric form has the desirable property that it obeys "action is minus reaction", i.e. the fact that momentum is conserved.

2.3 Gradient correction of the kernel function

Bonet and Lok [7] presented a method for the gradient correction of the smoothing kernel. Oger et al. [6] showed that this method can improve the accuracy of equation (16) to the second order. The simplest technique to obtain the corrected kernel gradient ∇W_{ab} involves introducing a correction matrix L_a:

$$\nabla W_{ab} = \mathrm{L}_a \nabla w_{ab} \tag{18}$$

where

$$\mathrm{L}_a = \left[\sum_{b \in N} V_b \nabla w_{ab} \otimes \left(\vec{x}_b - \vec{x}_a \right) \right]^{-1} \tag{19}$$

is the correction matrix of size $d \times d$ and d is the number of dimensions.

The use of this correction technique ensures that the gradient of any linear velocity field is more accurately evaluated. In addition, angular momentum will be preserved provided that the internal forces are derived from the variational principle. The SPH symmetrical forms of equation with gradient correction should give better results than the asymmetrical forms of equation which implicitly apply the law of conservation of momentum [6]. However, using this correction scheme in simulating problems with a pronounced turbulent free surface, where the preservation of characteristics is essential in order to preserve the robustness of numerical scheme, can produce less satisfactory outcomes [8].

3. Incompressible SPH method (ISPH)

Incompressible SPH method is based on the projection scheme to solve the Navier-Stokes equations and was developed by Chorin and Temam independently in the 1960s [9, 10].

In the projection method, the pressure that is needed to satisfy the incompressibility condition is obtained by projecting the velocity field on the solenoidal space. The method is based on the Helmholtz-Hodge decomposition, according to which any vector field $\vec{V}$ can be uniquely resolved into the sum of an irrotational (curl-free) vector field and a solenoidal (divergence-free) vector field. This implies that any such vector field $\vec{V}$ can be considered to be generated by a pair of potentials, a scalar potential and a vector potential:

$$\vec{V} = \nabla f + \vec{V}_{sol} \tag{20}$$

Because of $\nabla \cdot \vec{V}_{sol} = 0$ and $\nabla \times \nabla f = 0$, it follows that:

$$\nabla \cdot \vec{V} = \nabla^2 f = \Delta f \tag{21}$$

J. Bašić, N. Degiuli, A. Werner
Simulation of Water Entry and Exit
of a Circular Cylinder Using the ISPH Method

Equation (21) is known as Poisson's equation for the scalar function f. If the non-solenoidal vector field $\vec{V}$ is known, Poisson's equation (21) can be solved, and thus the solenoidal field $\vec{V}_{sol}$ can be obtained according to equation (20).

3.1 Classical projection method

Classical projection method [5], which is also called homogeneous (or non-incremental), solves the discretized form of equation (1) dividing it into two parts. In the first step, colloquially called prediction step, the intermediate state without pressure gradient is calculated. The intermediate particle position $\vec{x}^*$ and the velocity field $\vec{u}^*$ can be explicitly evaluated by the following equations:

$$\vec{x}^* = \vec{x}^n + \vec{u}^n \Delta t \tag{22}$$

$$\frac{\vec{u}^* - \vec{u}^n}{\Delta t} = \nabla\left(\nu \nabla \cdot \vec{u}^n\right) + \vec{g} \tag{23}$$

The second step, colloquially called projection step, is based on the equation which is analogous to equation (20), thus it follows that:

$$\frac{\vec{u}^{n+1} - \vec{u}^*}{\Delta t} = -\frac{1}{\rho}\nabla p^{n+1} \tag{24}$$

The pressure value is evaluated by taking the divergence of equation (24):

$$\nabla \cdot \left(\frac{\vec{u}^{n+1} - \vec{u}^*}{\Delta t}\right) = -\nabla \cdot \left(\frac{1}{\rho}\nabla p^{n+1}\right) \tag{25}$$

and satisfying the continuity equation (2), equation (25) can be written analogously to equation (21) as:

$$\nabla \cdot \left(\frac{1}{\rho}\nabla p^{n+1}\right) = \frac{\nabla \cdot \vec{u}^*}{\Delta t} \tag{26}$$

The above equation is known as pressure Poisson's equation. When the pressure field is obtained by solving equation (26), the velocity field, which is solenoidal, i.e. divergence-free, is obtained according to equation (24):

$$\vec{u}^{n+1} = \vec{u}^* - \left(\frac{1}{\rho}\nabla p^{n+1}\right)\Delta t \tag{27}$$

Finally, according to equation (3), the new particle position is expressed as:

$$\vec{x}^{n+1} = \vec{x}^n + \left(\frac{\vec{u}^{n+1} + \vec{u}^n}{2}\right)\Delta t \tag{28}$$

The boundary condition for velocity along the wall reads:

$$\vec{u}^{n+1} \cdot \vec{n}\big|_{\Gamma} = 0 \tag{29}$$

and, a homogeneous condition for pressure follows from equation (24):

$$\nabla p^{n+1} \cdot \vec{n}\big|_{\Gamma} = 0 \tag{30}$$

This is an artificial Neumann boundary condition for the pressure which is responsible for a numerical boundary layer on the pressure that limits the accuracy of the scheme [11]. This is a known issue and is not specific only for the SPH method. The use of higher-order time differentiation does not result in substantial accuracy improvement. For most problems, the classical method gives acceptable deviations, but for more complex simulations the physically consistent pressure boundary condition needs to be corrected to obtain a better approximation of the pressure.

4. Implementation

The following sections describe the proposed implementation of the ISPH method which involves the projection solving of the pressure and the velocity field, used SPH formulations, implementation of boundary conditions, time-advancing conditions and tensile instability.

4.1 SPH Formulation

The standard asymmetric form of the pressure gradient (17) ensures the preservation of momentum and automatically adjusts the particle positions. Thus, the pressure gradient is given as:

$$\left(\frac{1}{\rho}\nabla p\right)_a = \sum_{b\in N} m_b\left(\frac{p_a}{\rho_a^2} + \frac{p_b}{\rho_b^2}\right)\nabla W_{ab} \tag{31}$$

Divergence of the vector velocity field, which is necessary to solve the Poisson equation (26), is given in a symmetrical form as:

$$\nabla\cdot\vec{u}_a = \frac{1}{\rho_a}\sum_{b\in N} m_b\left(\vec{u}_b - \vec{u}_a\right)\cdot\nabla W_{ab} \tag{32}$$

Morris [12] approximated the factor of laminar viscosity combining the SPH method and finite difference method, using only the first derivative of the kernel function:

$$\nu\nabla^2\vec{u}_a = \frac{2\mu}{\rho_a}\sum_{b\in N} V_b\frac{\vec{x}_{ab}\cdot\nabla W_{ab}}{\left|\vec{x}_{ab}\right|^2 + \eta^2}\left(\vec{u}_a - \vec{u}_b\right) \tag{33}$$

where $\vec{x}_{ab} = \vec{x}_a - \vec{x}_b$ and η is a parameter of small value to avoid zero dominator, and its value is usually taken as $\eta = 0.1h$.

Analogously, the Laplace operator for pressure can be approximated as:

$$\nabla^2 p_a = 2\sum_{b\in N} V_b\frac{\vec{x}_{ab}\cdot\nabla W_{ab}}{\left|\vec{x}_{ab}\right|^2 + \eta^2}\left(p_a - p_b\right) \tag{34}$$

4.2 Boundary conditions

Due to the Lagrangian nature of the SPH method, implementation of boundary conditions is not straightforward as in the grid-based methods. Generally, there are three ways of how to treat rigid walls in the SPH method: repulsive force (repulsive particles), mirror particles, and dummy particles method.

For the repulsive force method, a single layer of fixed particles is set to the line of the wall. The particles have very strong repulsive forces to prevent the penetration of fluid

particles through the wall. This method cannot completely satisfy the homogeneous Neumann condition for the pressure [13].

The mirror particles method needs to determine virtual particles which are on the tangent to the boundary surface and this must be done in each time step. When the fluid particles are near the wall, virtual particles represent a reflection of real particles through the boundary. An approximation of no-slip condition can be achieved by giving the virtual particles the same density and pressure, but the opposite velocity to that of the near-wall fluid particles [12]. Continuous generation of particles complicates the parallel implementation and the modelling of complex, especially sharp concave shapes is a very demanding problem.

Koshizuka et al. [14] introduced a description of walls with dummy particles for the Moving Particle Semi-implicit method (MPS) and was later widely accepted for the ISPH method [15, 16, 17] since it gives more accurate results [18]. One layer of particles is set onto the wall line, and a few extra layers of dummy particles are placed within a rigid wall in order to implicitly impose the Neumann condition. Particles are generated at the beginning of the simulation, and laid in the opposite direction to the normal vector of the wall. They have the same values of pressure and velocity as well as the corresponding particles on the wall. The number of additional layers is determined by the radius of the kernel domain.

There is no standard method of generating dummy particles around curved walls or corners of the walls which most accurately imposes Neumann boundary condition. This represents a problem on which numerous researchers currently work [8, 17, 19, 20, 21]. Dummy particles on curved walls, as well as on the flat walls, are usually generated as shown in Figure 1. In the case of larger curvature it is necessary to keep the deviation of the distance between particles on the curve from the Euclidean distance as small as possible.
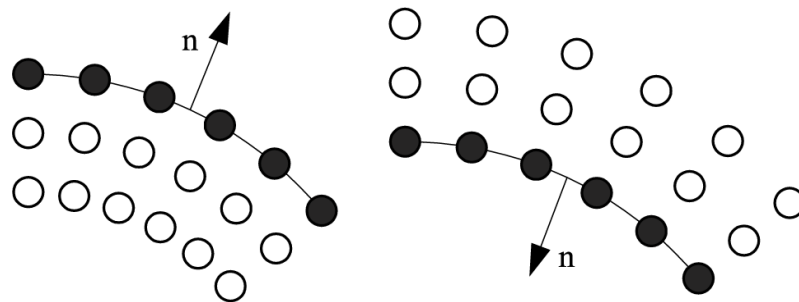

Fig. 1 Layout of dummy particles on curved walls (black - wall particles, white - dummy particles)

For an arbitrary angle in which flow occurs, the question is how to fill the void behind the coupling of two walls. Figure 2 shows the proposed method for the generation of particles over the arc angle between two normal vectors at the junction.

For an arbitrary angle around which flow occurs, there is a problem of dummy particle mixing on the connected walls. In this case, the centreline is taken as the boundary that divides dummy particles belonging to two walls.

Lastwika et al. [21] have implemented a genuine entry condition for compressible flows by attaching an inflow zone upstream of the computational domain. Particles within the inlet zone preserve their characteristics in order to meet the analytical boundary condition at the entrance.
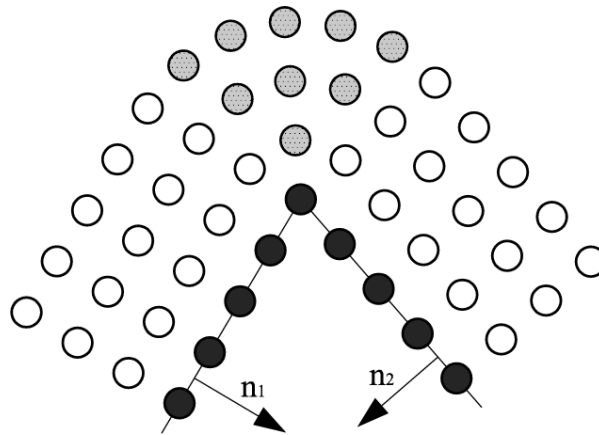
Fig. 2 Layout of dummy particles for concave angles

4.3 The pressure Poisson equation

Discretized form of the pressure Poisson equation (26), according to equations (32) and (34), forms a linear system of equations $\sum_{b \neq a} A_{ab}(p_a - p_b) = b_a$, respectively $\sum_{b} A_{ab} p_b = b_a$, which can be written as:

$$...p_b A_{ab} + ...p_a A_{aa} + ... + ...p_c (A_{ac} + A_{ad} + ...) = b_a \tag{35}$$

where a and b are the fluid particles, c is the particle on the boundary and d is the dummy particle having the same pressure as the particle c.

Linear system can be represented in a matrix form as $\mathbf{Ax} = \mathbf{b}$; according to equation (34), the coefficients of the matrix $\mathbf{A}$ for fluid particles are given by the expression:

$$\mathbf{A}_{ab} = \begin{cases} 2V_b \dfrac{\vec{x}_{ab} \cdot \nabla W_{ab}}{|\vec{x}_{ab}|^2 + \eta^2} & \text{for } a \neq b \\ -\sum_{b \in N} \mathbf{A}_{ab} & \text{for } a = b \end{cases} \tag{36}$$

and according to equation (32), the elements of the right-hand-side vector $\mathbf{b}$ are given as:

$$\mathbf{b}_a = \frac{\beta}{\Delta t} \sum_{b \in N} m_b \left(\vec{u}_b^* - \vec{u}_a^* \right) \cdot \nabla W_{ab} \tag{37}$$

4.3.1 Neumann boundary condition

As described in section 4.2, the Neumann boundary condition (29) is implicitly imposed using the particles of rigid walls and dummy particles. Dummy particles participate in all SPH formulations for fluid particles, but the pressure value of these particles is not calculated in the solution of Poisson equation. Particles of rigid walls are included in the system of linear equations and the form of matrix coefficients is the same as that for the fluid particles, except for the fact that they consider only the interaction with fluid particles. After solving the pressure from the Poisson equation in the positions of fluid and rigid walls particles, dummy particles take pressure values from the matching rigid wall particles. Thus, dummy particles have an important impact in the calculation of the pressure gradient in equation (31), and the vector velocity field becomes divergence-free using equation (27).

4.3.2 Dirichlet boundary condition

When simulating flows with free surface, the Dirichlet condition $p = 0$ should be imposed on particles that have been identified as free surface particles, so that the system has a nontrivial solution. This condition can be strictly achieved by the following simple modification in the linear system for free surface particles:

$$\mathbf{A}_{ab} = \begin{cases} 0 & \text{for } a \neq b \\ 1 & \text{for } a = b \end{cases} \tag{38}$$

$$\mathbf{b}_a = 0$$

However, Bøckmann et al. [22] proposed a less strict implementation of the Dirichlet condition in order to improve the properties of the formulation of pressure gradient (31) and to avoid the accumulation of small groups of particles near the free surface. From the Dirichlet condition $p_a = 0$ and equation (34), it follows that:

$$\varepsilon \cdot p_a \cdot 2 \sum_{b \in N} V_b \frac{\vec{x}_{ab} \cdot \nabla W_{ab}}{\left|\vec{x}_{ab}\right|^2 + \eta^2} = 0 \tag{39}$$

From the sum of equations (40) and (45), the constant ε should determine the relative importance of satisfying the Dirichlet condition in the system (26). It has been shown by empirical research that $\varepsilon = 1$ gives satisfactory results [22]. Therefore, the free surface particles have a modified diagonal of the coefficient matrix $\mathbf{A}$, as follows:

$$\mathbf{A}_{aa} = -2 \sum_{b \in N} \mathbf{A}_{ab} \tag{40}$$

Fluid boundary is determined by the value $\nabla \cdot \vec{r}$ without the correction of kernel function gradient:

$$\nabla \cdot \vec{r} = \sum_{b \in N} V_b \left(\vec{x}_a - \vec{x}_b\right) \cdot \nabla w_{ab} \tag{41}$$

For the free-surface particles in the 2D case, equation (41) gives values near 2.0, and for the 3D case values near 3.0. For particles that are close to the free surface, calculated values are lower than the specified ones. Standard marginal values for testing are 1.5 and 2.4 for 2D and 3D cases, respectively. Although this method is not absolutely precise, an improper free-surface classification for a minor amount of particles does not result in significant deviations in the final results.

4.4 Time advancing

Stability simulation depends on the time step Δt, which can be variable, but it should neither be too large nor too small. It depends on the CFL and the viscosity condition:

$$\Delta t \leq \min(\Delta t_{CFL}, \Delta t_v) \tag{42}$$

Maximum allowable time step Δt_{CFL}, which depends on the CFL condition is given by:

$$\Delta t_{CFL} = 0.2 \frac{\lambda}{u_{max}} \tag{43}$$

where u_{max} is the value of the maximum fluid velocity, namely the velocity of the fastest particle.

Maximum allowable time step Δt_ν, which depends on the viscosity is given by:

$$\Delta t_\nu = 0.125 \frac{h^2}{\nu_{max}} \tag{44}$$

where ν_{max} is the maximum effective kinematic viscosity in the simulation, and for the isothermal flow $\nu_{max} = \nu = \text{const.}$

4.5 Tensile instability

The particles move along the streamlines when the Navier-Stokes equations are exactly solved. Therefore, it is reasonable to presume that the accumulation of particles will take place in the vicinity of the stagnation points of fluid flow, which normally occurs in the area of negative pressure and sometimes in other cases. This instability is caused by the defect of the kernel functions and it results in interpolation errors [23, 24]. According to the first derivative of the kernel function, the closing-in of the particles up to a certain distance results in a weaker mutual influence, rather than a stronger one. Xu [16] proposed a method of correcting the particle which has previously been introduced in the finite volume particle method (FVPM). The particle shift vector to the corrected position is given by the equation:

$$\delta \vec{r}_a = C |\vec{u}_a| \Delta t \left(\vec{r}_a^2 \sum_{b \in N} \frac{\vec{n}_{ab}}{r_{ab}^2} \right) \tag{45}$$

where C is the arbitrary chosen constant, usually in the interval [0.01; 0.1], $\vec{n}_{ab}$ is the normalized vector between the position of particles a and b, and $\vec{r}_a$ is the averaged distance of particles in the neighbourhood of the particle a, given by:

$$\vec{r}_a = \frac{1}{N} \sum_{b \in N} r_{ab} \tag{46}$$

From the finite set of particles near the free surface, only particles whose distance from the surface is less than the averaged neighbourhood distance should be taken into account in equations (45) and (46).

After correction of the particle positions in the fluid domain, it is necessary to interpolate the hydrodynamic variables. Pressure and velocity vector components can be corrected by the Taylor expansion:

$$f_{a'} = f_a + (\nabla f)_a \cdot \delta \vec{r}_a + O(\delta r_a^2) \tag{47}$$

where f is the scalar field of pressure or velocity components.

The previously mentioned redistribution of particles and the correction of hydrodynamic variables can result in the "jump" of particles from one streamline to another, thus avoiding the accumulation of particles into groups as shown in Figure 3, also reducing the error caused by the perturbed distribution of distance between particles.
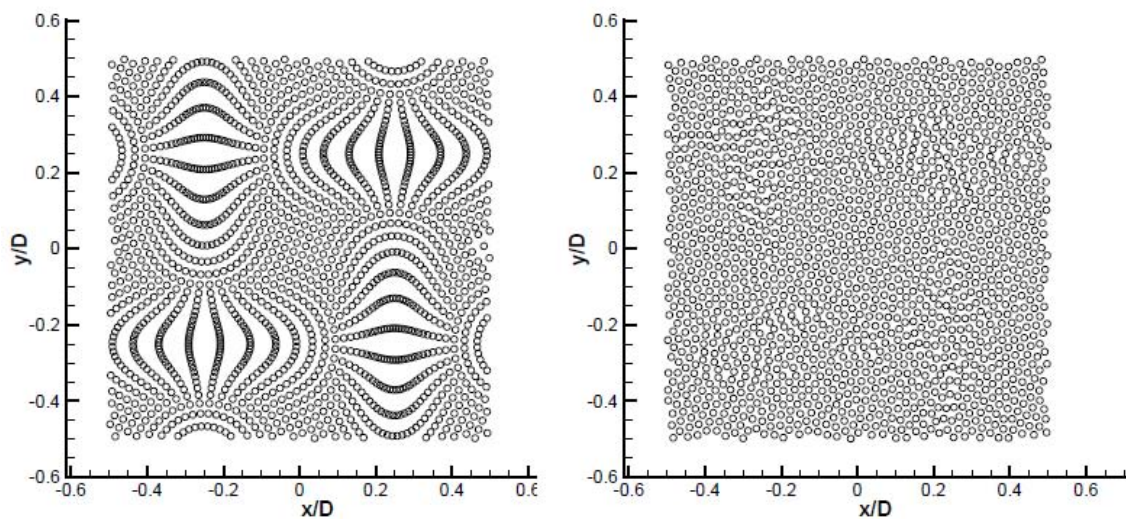
Fig. 3 Distribution of particles in the simulation of Taylor-Green vortices with and without correction of the particle positions [16]

5. Verification and validation

The tests by which the current 2D implementation of the ISPH method has been verified and validated are described below. Simulation results were compared with analytical and experimental results available in the literature. Tests were simulated using a classical homogeneous projection scheme. Gradient correction of smoothing kernel functions was not used, while the correction of the particle positions, described in section 4.5, was used when the negative pressure field occurred. Spline kernel function of the fifth order was used with the smoothing length of $h = 1.2\lambda$.

5.1 Water entry and exit of a circular cylinder

This section presents numerical simulations of two dimensional water entry and exit of a circular cylinder at a forced constant velocity. The water exit of a rigid body immersed in fluid is a problem that is less studied than the forced water entry. The water entry phase of a rigid body includes the so-called slamming effect. This problem may be associated with the formation of air pockets and local hydroelastic effects. In a very small time interval, when generating air pockets, compressibility of the air is important, but it generally does not affect the response of the rigid structure. Gravity and viscosity have a negligible impact during the initial water entry phase, but they become essential in the later phases or during the water exit.

The ISPH method was compared with the experiments conducted by Miao [25] in 1989 at the Marine Technology Centre in Trondheim. The tank is 28 m long, 2.5 m wide and has a water depth of 1.0 m. A PVC cylinder with a diameter of $D = 0.125\,\mathrm{m}$ and a length of $L = 0.25\,\mathrm{m}$ was used for the impact force measurement. In order to achieve a two dimensional flow condition, the model was equipped with two wide plexiglas plates. A hydraulic system towed the model vertically downwards into water with velocities ranging from 0 to about the maximum velocity $U = 2.66\,\mathrm{m/s}$.

Figure 4 shows the scheme for water entry and Figure 5 for water exit of a circular cylinder with constant velocity according to which the numerical simulations were modelled.
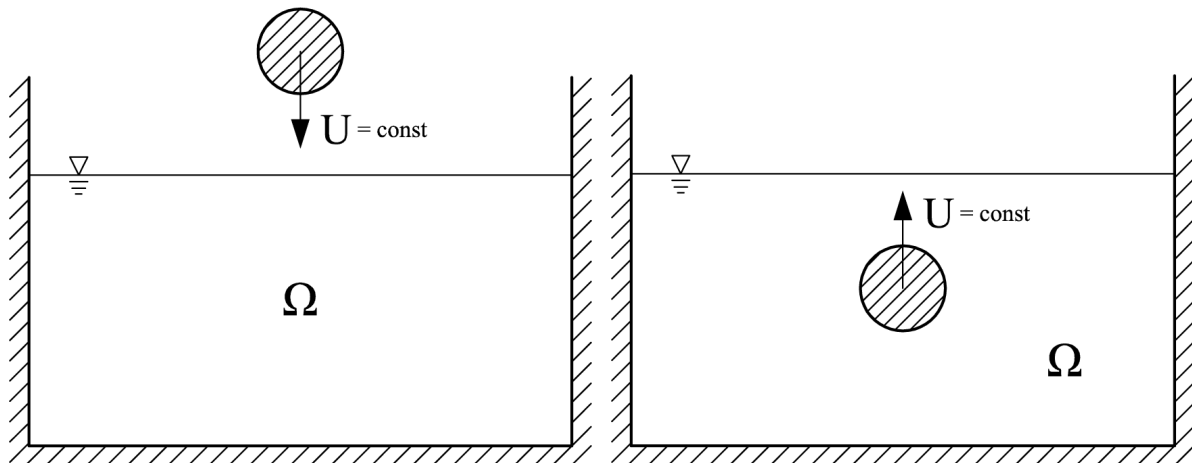
Fig. 4 Schematic representation of water entry test of a circular cylinder with constant velocity

Fig. 5 Schematic representation of water exit test of a circular cylinder with constant velocity

5.1.1 Water entry of a circular cylinder at a constant velocity

Two tests were performed for comparison with the experiments, and were characterized by defined constant velocities of water entry given in Table 1.

Table 1 Parameters of the cylinder water entry tests at a constant velocity

Experiment no.	1	2
Velocity U, m/s	0.5124	0.876

Dimensionless impact force C_s, the so-called slamming coefficient, is defined by the following equation:

$$C_s = \frac{F_y}{\frac{1}{2}\rho U^2 2r} = \frac{F_y}{\rho U^2 r} \tag{48}$$

where r is the radius of cylinder and F_y the total vertical hydrodynamic force per unit length of the cylinder, which is the cause of water entry and includes the buoyancy. Possible parameters affecting the impact force are the Froude and the Reynolds number, the surface roughness of the cylinder and the Euler, the Weber, and the Cauchy number. The Weber and the Cauchy number are related to the surface tension and the compressibility of the fluid, respectively. Surface tension becomes important when describing the free surface of greater curvature, such as spray or bubble, which does not significantly affect the structural hydrodynamic load and is ignored along with the compressibility of the fluid. The Froude number dependence is both due to the free surface wave generation at the water entry of a cylinder and the buoyancy force. The Reynolds number has little effect on the results because the major vortices are concentrated in the boundary layer of the cylinder.

Numerical simulations were carried out in the tank with a width of 0.6 m and a depth of 0.4 m. Simulation consisted of 10500 particles with an initial spacing of $\lambda = 0.005$ m. Figure 6 shows the pressure field and the free surface deformation. After the impact of the cylinder on the free surface, two waves are developed and an open air cavity is created while the cylinder enters the water. The air cavity gradually closes and the collision between two free surfaces forms a short-term bump. The maximum value of force occurs when the cylinder is immersed in water immediately after the closing of the open air cavity.
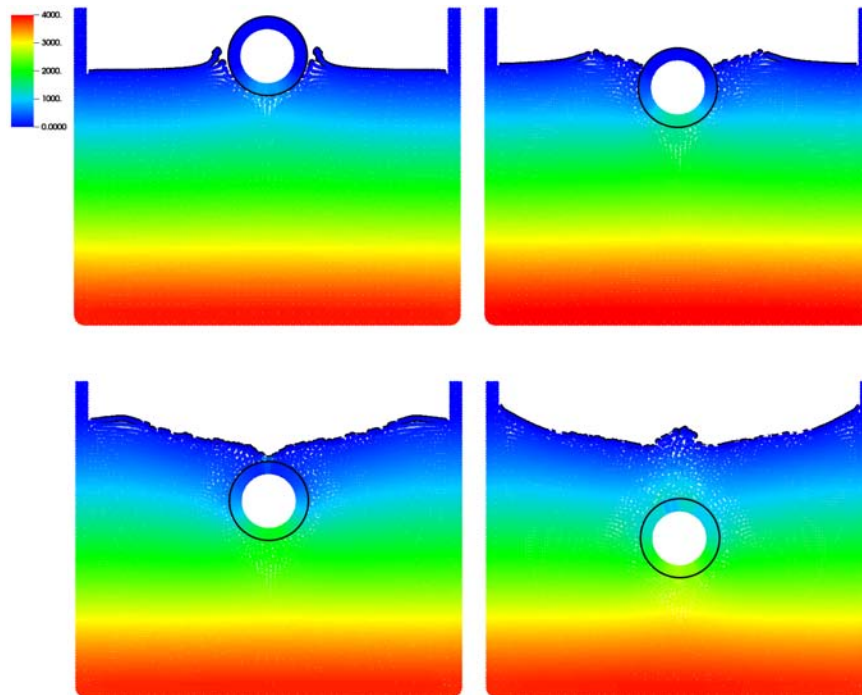
Fig. 6 Simulation of the cylinder water entry, experiment no. 1, $U = 0.5124$ m/s [26]

Figures 7 and 8 show the dimensionless force acting on the cylinder as a function of dimensionless time tU/r. Force values obtained by the ISPH method, regardless of the fluctuations that are caused by oscillations of the pressure field with the increase in theFroude number are very close to the experimental values. Oscillation of pressure fields can be reduced through a better selection of input parameters for simulation, such as reducing the particle spacing λ, the smoothing length h and the time step Δt.

However, there are also some experimental errors due to buoyancy and friction forces of plates at the cylinder ends, the 3D flow effects, and hydroelastic effects.
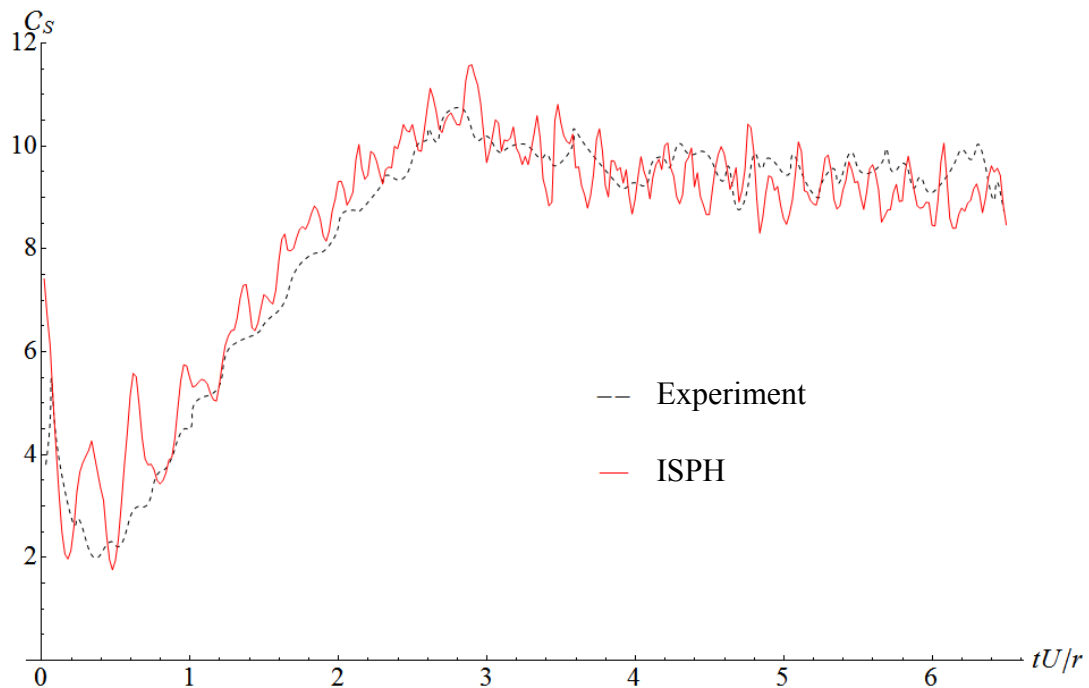

Fig. 7 Dimensionless slamming coefficient for experiment no. 1, $U = 0.5124$ m/s. Comparison between the results obtained with the ISPH method [26] and those obtained experimentally [25].
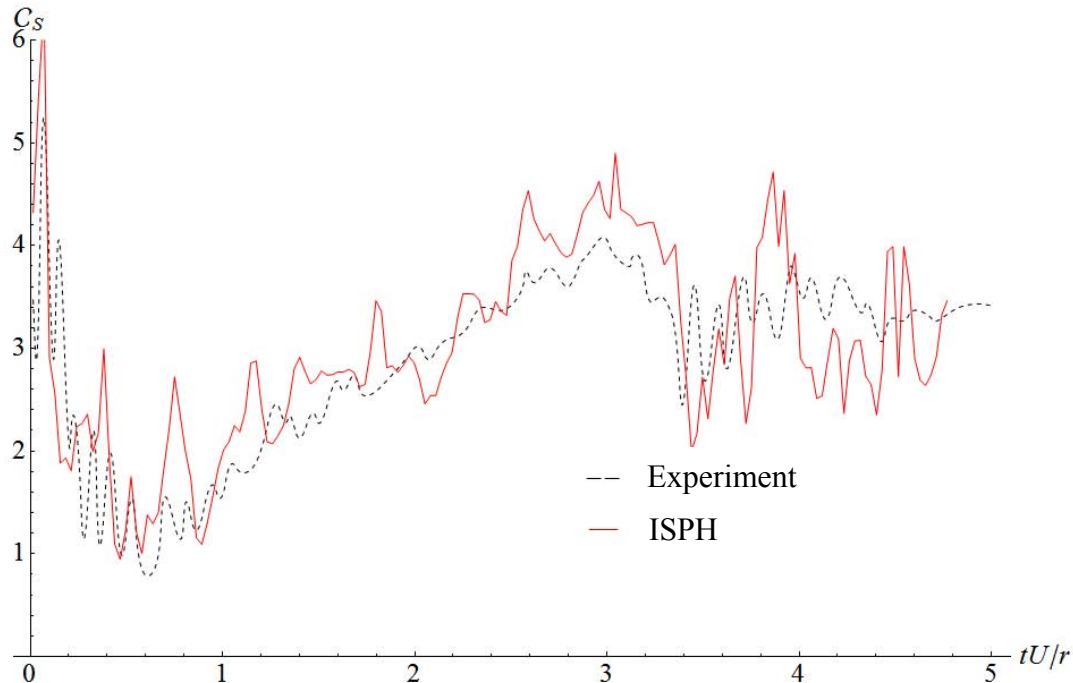
Fig. 8 Dimensionless slamming coefficient for experiment no. 2, $U = 0.876$ m/s. Comparison between the results obtained with the ISPH method [26] and those obtained experimentally [25].

5.1.2 Water exit of a circular cylinder at a constant velocity

Water exit calculation was carried out for one test case and compared with the experiment characterized by a constant velocity $U = 0.5124$ m/s. Criterion for result comparison is the dimensionless force on the cylinder C_e, defined in the same way as the slamming coefficient C_s with equation (48). Experimental readings oscillate, which is probably associated with vibrations of the test rig that induce hydrodynamic added mass and structural inertia forces on the test cylinder. Vibrations are probably associated with the hydraulic system that works on the principle of displacement, and small deviations cause excessive acceleration. Zhu [27] proposed a simplified model to obtain the vertical force on the cylinder. The model does not take into account the free surface and is valid at times when the cylinder is not even close to the free surface. The values of force obtained by the ISPH method were compared with the experimental and analytical ones. Figure 10 shows the dimensionless force acting on the cylinder.

Numerical model of the cylinder accelerates vertically and uniformly to the characteristic velocity. To enable the use of a larger time step and to improve the flow around a cylinder, the particle position correction and the increased viscosity of water were used, as described in section 4.5. Particle position correction and excessive time step caused the simulation to lose stability for a brief moment that did not significantly affect the overall results of the force on the cylinder since the non-incremental projection method is used. Although numerically obtained values are slightly higher than the reference values due to the high viscosity, the good agreement of results is evident. Figure 9 shows the pressure field and the free surface deformation. As the cylinder approaches the free surface, the fluid above the cylinder rises progressively by reducing the radius of curvature to the radius of the cylinder. When the cylinder exits the water, the water surface continues to flow vertically for a short time.
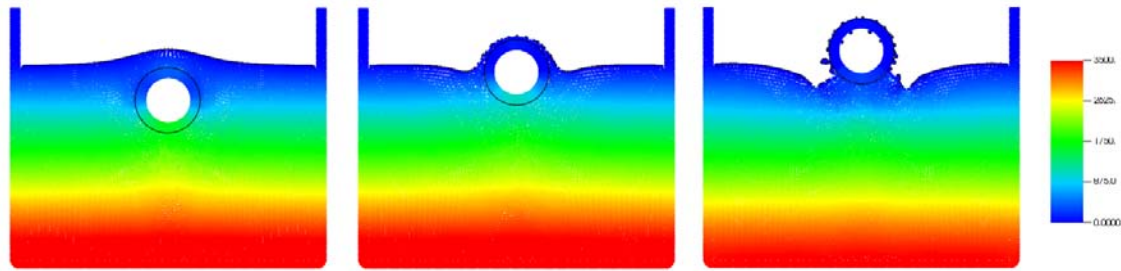
Fig. 9 Simulation of the cylinder water exit, experiment no. 1, $U = 0.5124$ m/s [26]

6. Conclusions

The study presents the incompressible smoothed particle hydrodynamics (ISPH) method, a numerical method for simulating the dynamics of an incompressible viscous fluid based on a system of particles. Compared to the classical SPH method, ISPH is based on the projection scheme to solve the Navier-Stokes equations. The advantage of the implicit-explicit scheme is the ability to use a larger time step, and the resulting pressure and velocity fields are smoother compared to those obtained using explicit SPH methods.

A computer program was developed, and the verification and validation of the proposed model was performed by simulating the problems for which the analytical or experimental data are already known. Two types of simulation were performed: water entry and water exit of a circular cylinder at a forced constant velocity. The obtained numerical results were compared with experiments conducted by Miao [25] and very good agreement was obtained.
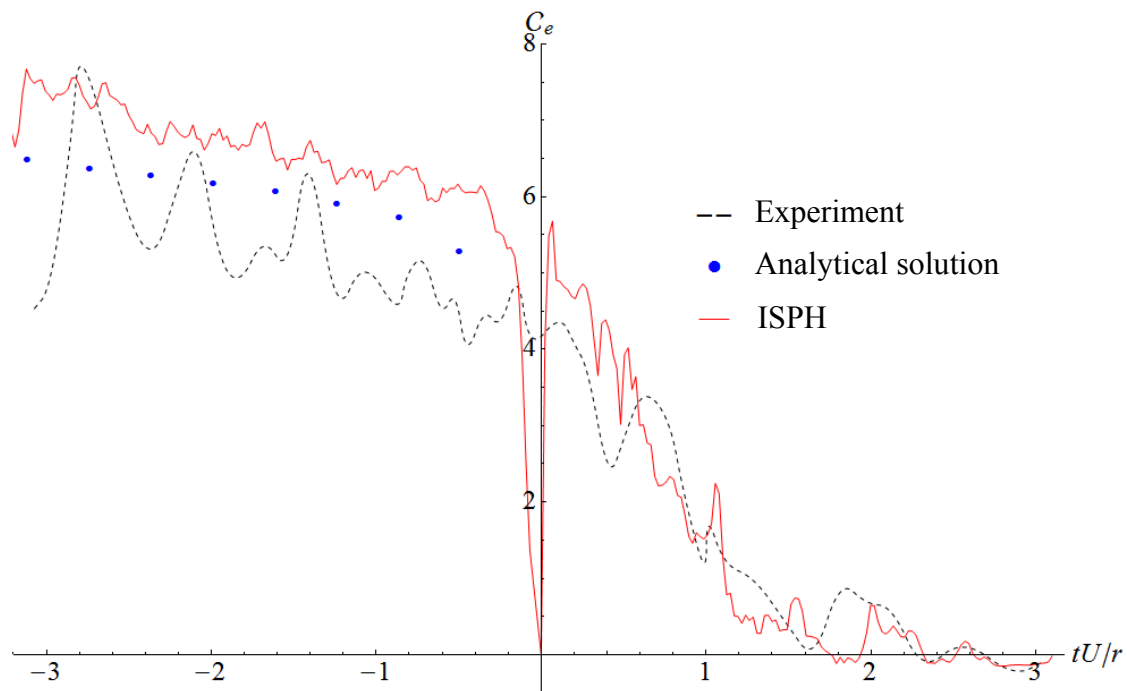

Fig. 10 Dimensionless force on the cylinder for experiment no. 1, $U = 0.5124$ m/s . Comparison between the results obtained with the ISPH method [26] and those obtained experimentally [25] and analytically [27].

It is shown that the ISPH method can preserve the total volume of fluid with sufficiently small time steps that satisfy the CFL condition. It is worth noting that excessively small time steps can cause fluctuations in the pressure field. The time step can be reduced to strive towards zero, but it is consequently necessary to reduce the distance between particles.

Implementation of boundary condition is not straightforward and boundary conditions for the SPH method are still an active area of research, since there are difficulties in imposing the homogenous Neumann boundary condition on complex geometries. Also, for the simulation of complex flows, the introduction of some turbulent model should be considered, which was not considered in this paper.

With a good selection of input parameters, the ISPH method can be stable for a number of different problems and thereby can provide accurate solutions with a smooth pressure and velocity fields. The Lagrangian nature of ISPH makes it convenient for simulating free surface flows in cases with large deformations and problems involving the interaction of solids and fluids with a free surface.

The ISPH method has the potential to become an attractive choice for solving fluid dynamics problems where the classical Euler method encounters difficulties, especially in marine hydrodynamics, where violent flows and violent fluid-structure interaction problems such as wave breaking, sloshing, green water, and water impact can occur. Future tests to continue the validation of the investigated method comparing it with semi-analytical and experimental results should include the water entry of a wedge, water entry of ship sections (bow flare and V-shaped section), and a simulation of a 3D ship motion with water on deck. Due to its explicit simplicity, the WCSPH method is already widely used for 3D simulations where an accurate prediction of hydrodynamic fields is not of great significance. But similarly to WCSPH, extending the 2D ISPH solver to solve 3D problems is straightforward. The extra performance cost of the ISPH implicit steps of the ISPH is virtually cancelled with time steps that are significantly larger than in the WCSPH method.

REFERENCES

[1]   Lucy, L.B.: "A numerical approach to the testing of the fission hypothesis", The Astronomical Journal, Volume 82, Issue 12, pp. 1013-1024, 1977.

[2]   Gingold, R.A., Monaghan, J.J.: "Smoothed particle hydrodynamics - Theory and application to non-spherical stars", Monthly Notices of the Royal Astronomical Society, Volume 181, pp. 375-389, 1977.

[3]   Monaghan, J.J.: "Smoothed particle hydrodynamics", Annual review of astronomy and astrophysics, Vol. 30, pp. 543-574, 1992.

[4]   Monaghan, J.J.: "Simulating Free Surface Flows with SPH", Journal of Computational Physics, Volume 110, Issue 2, pp. 399-406, 1994.

[5]   Cummins, S.J., Rudman, M.: "An SPH Projection Method", Journal of Computational Physics, Volume 152, Issue 2, pp. 584-607, 1999.

[6]   Oger, G., Doring, M., Alessandrini, B., Ferrant, P.: "An improved SPH method: Towards higher order convergence", Journal of Computational Physics, Volume 225, Issue 2, pp. 1472-1492, 2007.

[7]   Bonet, J., Lok, T.S.L.: "Variational and momentum preservation aspects of Smooth Particle Hydrodynamics formulations", Computer Methods in Applied Mechanics and Engineering, Volume 180, Issues 1-2, pp. 97-115, 1999.

[8]   Marrone, S.: "Enhanced SPH modeling of free-surface flows with large deformations", PhD thesis, University of Rome, La Sapienza, 2011.

[9]   Chorin, A.J.: "Numerical solution of the Navier–Stokes equations", J. Math. Comp., Volume 22, 1968.

[10]   Temam, R.: "Une méthode d'approximation des solutions des equations Navier-Stokes", Bull. Soc. Math. France, Volume 98, pp. 115–152, 1968.

[11]   Guermond, J.L., Minev, P., Shen, J.: "An overview of projection methods for incompressible flows", Computer Methods in Applied Mechanics and Engineering, Volume 195, Issues 44-47, pp. 6011-6045, 2006.

[12]   Morris, J.P., Fox, P.J., Zhu, Y.: "Modeling Low Reynolds Number Incompressible Flows Using SPH", Journal of Computational Physics, Volume 136, Issue 1, pp. 214-226, 1997.

[13]   Dalrymple, R.A., Rogers, B.D.: "Numerical modeling of water waves with the SPH method", Coastal Engineering, Volume 53, Issues 2-3, pp. 141–147, 2006.

[14] Koshizuka, S., Nobe, A., Oka, Y.: "Numerical Analysis of Breaking Waves Using the Moving Particle Semi-Implicit Method", International Journal for Numerical Methods in Fluids, Volume 26, Issue 7, pp. 751–769, 1998.

[15] Shao, S., Lo, E.: "Incompressible SPH method for simulating Newtonian and non-Newtonian flows with free surface", Advances in Water Resources 26, pp. 787–800, 2003.

[16] Xu, R.: "An Improved Incompressible Smoothed Particle Hydrodynamics Method and Its Application in Free-Surface Simulations", PhD thesis, University of Manchester, Faculty of Engineering and Physical Sciences, 2009.

[17] Lee, E.S., Moulinec, C., Xu, R., Violeau, D., Laurence, D., Stansby, P.: "Comparisons of weakly compressible and truly incompressible algorithms for the SPH mesh free particle method", Journal of Computational Physics, Volume 227, Issue 18, pp. 8417–8436, 2008.

[18] Dong, T., Jiang, S.: "Comparisons of Mirror and Static Boundary Conditions in Incompressible Smoothed Particle Hydrodynamics", International Conference on Computational and Information Sciences (ICCIS), Chengdu, Sichuan China, 2010.

[19] Børve, S.: "Generalized Ghost Particle method for handling reflecting boundaries", 6th International SPHERIC Workshop, Hamburg, 2011.

[20] Yildiz, M., Rook, R.A., Suleman, A.: "SPH with the multiple boundary tangent method", International Journal for Numerical Methods in Engineering, Volume 77, Issue 10, pp. 1416-1438, 2009.

[21] Lastiwka, M., Basa, M., Quinlan, N.J.: "Permeable and Non-reflecting Boundary Conditions in SPH", International Journal for Numerical Methods in Fluids, Volume 61, Issue 7, pp. 709-724, 2009.

[22] Bøckmann, A., Shipilova, O., Skeie, G.: "Incompressible SPH for free surface flows", Computers & Fluids, Volume 67, pp. 138–151, 2012.

[23] Swegle, J.W., Hicks, D.L., Attaway, S.W.: "Smoothed Particle Hydrodynamics Stability Analysis", Journal of Computational Physics, Volume 116, Issue 1, pp. 123-134, 1995.

[24] Monaghan, J.J.: "SPH without a Tensile Instability", Journal of Computational Physics, Volume 159, Issue 2, pp. 290–311, 2000.

[25] Miao, G.: "Hydrodynamic Forces and Dynamic Responses of Circular Cylinders in Wave Zones", PhD. thesis, Department of Marine Hydrodynamics, NTH, Trondheim, Norway, 1989.

[26] Bašić, J.: "Metoda hidrodinamike izglađenih čestica za dinamičku simulaciju nestlačivog strujanja", Diplomski rad, Fakultet strojarstva i brodogradnje, Zagreb, 2012.

[27] Zhu, X.: "Application of the CIP Method to Strongly Nonlinear Wave-Body Interaction Problems", PhD thesis, Norwegian University of Science and Technology, Trondheim, 2006.

Josip Bašić
jbasic@live.com
Nastia Degiuli
nastia.degiuli@fsb.hr
Andreja Werner
andreja.werner@fsb.hr
Faculty of Mechanical Engineering and
Naval Architecture,
University of Zagreb,
Ivana Lučića 5,
10000 Zagreb, Croatia